Hydrosedimentary monitoring of the Hydrothiem observatory, Eastern tropical coast of New Caledonia (SW Pacific)

Pierre Genthon [a,*], Caroline Tramier [a,b,d], Quentin Delvienne [c], Pascal Dumas [d], Nathalie Rouché [e], Kavya Wijesuriya [a], Jean-Jerôme Cassan [b], Angelline Goué [b,1]

[a] *HydroSciences Montpellier, University of Montpellier, French Institute for Research for Development (IRD), Nouméa, New Caledonia*
[b] *Northern Province, Koné, New Caledonia*
[c] *French International Forest Office (ONFI), Saint Mandé, France*
[d] *UMR 228 ESPACE-DEV, University of New Caledonia (UNC), French Institute for Research for Development (IRD), Nouméa, New Caledonia*
[e] *HydroSciences Montpellier, University of Montpellier, French National Research Institute for Sustainable Development (IRD), CNRS, Montpellier, France*

ABSTRACT

Study region: The eastern coast of New Caledonia (SW Pacific).
Study focus: The HydroThiem hydrological observatory is devoted to the study of the impact of invasive ungulate species and bushfires on water resources, erosion and water quality in a catchment used for drinking water. It includes (1) three 100 m^2 plots located on characteristic land surfaces, i.e. a woody savanna submitted to bushfires every few years, a healthy forest and a forest strongly degraded by deer and wild pigs, (2) two watersheds covering areas of 25 200 m^2 and 3.1 km^2. The first watershed includes mostly savanna while the second one is mostly constituted of humid forest. Available data include rainfall, soil moisture, discharge, and suspended matter concentration.
New hydrological insight: Discharge and erosion rates exhibit striking differences between the three plots: the healthy forest presents a 3 % runoff and almost no erosion, the degraded forest being characterized by a 90 % runoff and large erosion, the savanna presenting intermediate values of runoff and erosion. The largest watershed present a 64 % runoff and an erosion rate amounting to 72 % of the one of the degraded plot. This emphasizes the role of subsurface flow and of gully erosion, respectively. Results from the Hydrothiem observatory can be used for a comparison with similar watersheds and may suggest guidelines for restoration and conservation strategies.

1. Introduction

Wildfires are a general concern worldwide. Recently, emphasis was set on giant wildfires and their immediate and long term environmental consequences (Duncombe, 2020), especially on the hydrosedimentary regime of burned surfaces (Viera et al., 2015; Stavi, 2019; Ebel et al., 2022). Besides, stable patterns of forest and savanna may be maintained in the tropics by frequent and low severity fires due to tree cover-fire feedbacks (Murphy and Bowman, 2012). Contrasted soil properties result from gradation in fire

---

severity (Mataix-Solera et al., 2011; Moody et al., 2016) which also result in contrasted hydrosedimentary responses to fire (Moody et al., 2013). The East coast of New Caledonia (SW Pacific) presents a high frequency of human induced fires – termed locally as bushfires – which constitute a common agricultural practice near villages and a space management tool for hunting activities (Toussaint, 2020). More than 70 % of bushfires occur at less than 0.5 km from an access road or an house (Dumas et al., 2013) and it is estimated by local people that each surface located a few km away from a road or a village is burned every 3 yrs. This produces a woody savanna land surface, characterized by an herbaceous strata including mostly invasive species and an unique and fire resistant woody species, *Melaleuca quinquenervia* (Ibanez et al., 2013). As a consequence of seeds dispersal and fire dynamics, savannas are present near crest lines (Ibanez et al., 2013) and may impact the hydrosedimentary regime of forests located downstream (Tramier et al., 2021).

In New Caledonia the population of deer (*Cervus timorensis*) and of wild pigs (*Sus scrofa*) has dramatically increased for the last 30 years and they are now considered as a threat to forests (de Garine-Wichatitsky et al., 2009). Deer browse the regeneration strata and wild pigs scour the soil. Impacts of deer on forests equilibrium are a general concern (Martin and Baltzinger, 2002; Davis et al., 2016). As invasive ungulate species impact soil and root properties, consequences are expected on the hydrological regime of degraded surfaces. However, very few studies dealt with effects of ungulate species on the hydrological and erosion regime of forests (Nakagawa, 2021).

The HydroThiem observatory is devoted to hydrological studies of individual surfaces degraded by low intensity wildfires and by invasive ungulate fauna by comparison with a healthy forest surface as well as with a mosaic of such surfaces at the scale of a small catchments. Since the setup of this observatory in 2017, it produced an unprecedented dataset in the Southern Pacific region allowing an understanding of flow generation and erosion at the scale of erosion plots and small catchments. Data recorded between 0ct. 2018 and March 2021 are presented, including rainfall, discharge, suspended matter concentration (SMC), erosion and soil moisture. These data could be useful for researchers working on impacts of fire and of ungulate invasive fauna as well as for comparison of different examples of tropical forests and savannas.

2. Study area

The HydroThiem hydrological site is located near the village of Touho, on the windward coast of Grande Terre, the main island of New Caledonia (SW Pacific) in the 64 km^2 watershed of the Thiem river (Fig. 1). It is included in the Massif des Levres, which is the second largest massif in Grande Terre culminating at 1076 m altitude. The Thiem river drains in the lagoon surrounding Grande Terre which is a hot spot of biodiversity and one of the world heritage sites of UNESCO. Climate is wet tropical with a marked rainy and warm
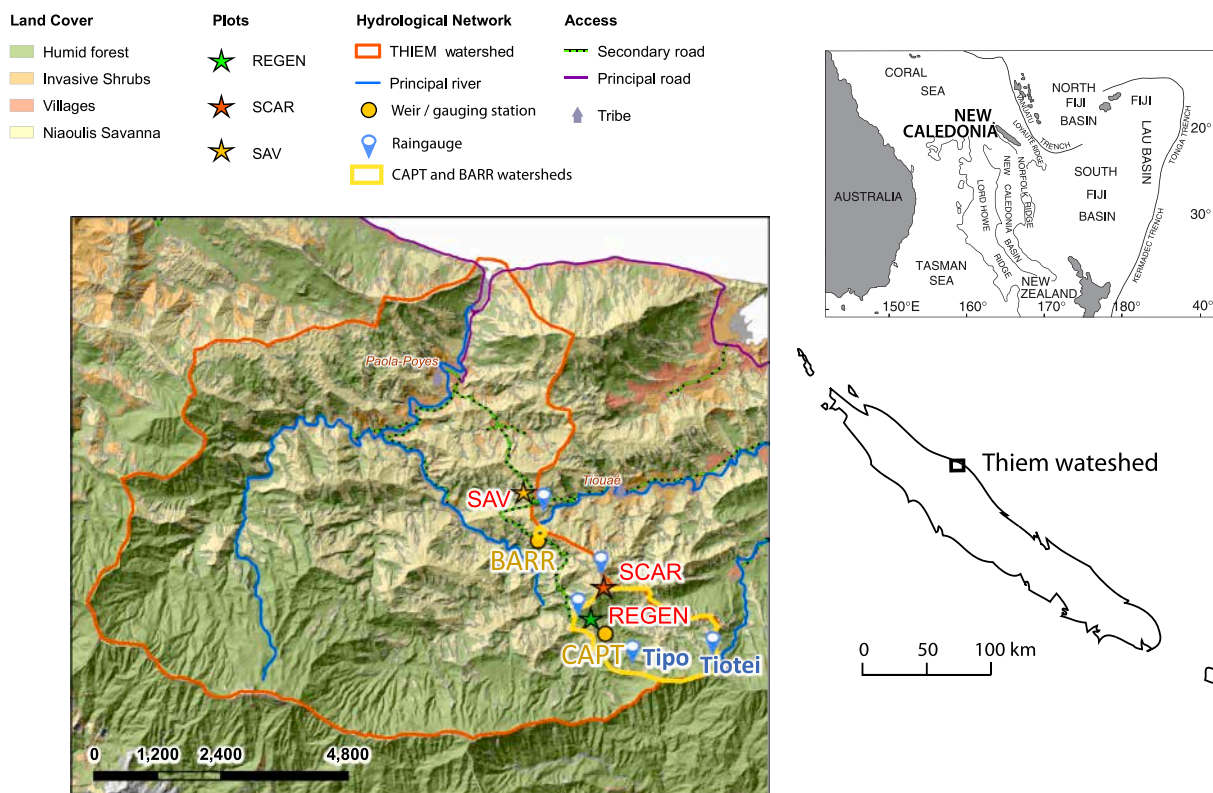
Fig. 1. Study area with location of the different hydrological features and equipment. The BARR watershed is located immediately to the north of the BARR gaging station.

season, between December and March, and a drier and cooler season between June and September. Rainfall is strongly modulated by ENSO (El Niño Southern Oscillation); El Niño years are dryer, while La Niña corresponds to humid years. During the wet season, the study area is exposed to tropical depressions and cyclones, with rainfall amounting to several hundred of mm in a few days (Maitrepierre, 2012). Temperature variations are limited all year long and the mean annual rainfall at zero altitude is 2400 mm (Fig. 2).

The basement consists of low temperature/high pressure metasediments with limited outcrops of ultramafic serpentines (less than 10 % in area), generally corresponding to crest lines (Maurizot et al., 2020). This basement is topped with a weathering profile characteristic of a humid tropical climate. There are only poor data on the weathering profile of micaschists of Grande Terre (Maurizot et al., 2020), but it is expected to correspond to the general pattern of weathering of basement rocks and to include from top to bottom: an organic layer (layer b), a lateritic layer, up to a few tens meter thick and including clay minerals according to the composition of the parent rocks, a saprolitic layer where fragments of the original parent rock can be recognized, and finally at the base of the profile a fissured layer, up to a few tens meter thick (Lachassagne et al., 2021). Both the superficial organic layer and the fissured layer present significant permeability.

3. Instrumentation

Data were recorded at three 100 m² hydrosedimentary plots – SAV, REGEN and SCAR – and at two small catchments – BARR and CAPT –, which are indicated in Fig. 1 and described in Sections 3.2 and 3.3. The type of data recorded at each plot or catchment is indicated in Table 1 and each data type is discussed below.

3.1. Rainfall

Five automatic tipping bucket raingauges were installed. SAV, REGEN and SCAR are equipped with Campbell CS 701 raingauges, which allow to record rainfall with a 2 % accuracy for intensities in the 0–250 mm/h range and a 3 % accuracy in the 250–500 mm/h range. Rainfall data were recorded at a 6 min time step by CR 200X data loggers. These three raingauges were calibrated in the field in 2019 and 2021 according to the manufacturer's specifications and rainfall data are available continuously between May 2018 and Oct. 2021. Two additional Onset RG3-M raingauges were installed in the upper CAPT watershed and called Tipo and Tiotei. Their accuracy is 1 % up to a rainfall intensity of 130 mm/h and they were calibrated in the laboratory before installation in Feb. 2020. Due to power shortages and failures, only discontinuous records are available for these two raingauges. Altitudes of the five raingauges are 190 m, 220 m, 345 m, 370 m, and 400 m for SAV, REGEN, Tipo, Tiotei and SCAR, respectively, with an accuracy of 10 m. No corrections were applied to rainfall data. Cumulated rainfall from the SAV, SCAR and REGEN raingauges are pictured in Fig. 3.

3.2. Runoff, soil moisture suspended matter and erosion at the plot scale

3.2.1. Runoff

Three plots were installed in contrasted land surfaces, with a similar area near 100 m² (20 m × 5 m) and along similar slopes. These three plots were described in Tramier et al. (2021) and their major features are listed in Table 2. The SAV plot (Fig. 4a) is located in a woody savanna, which was subjected to a bushfire in Oct. 2015 according to local inhabitants. This plot was burned again by our team in Oct. 2019 and allowed to recover spontaneously since then. The REGEN plot (Fig. 4b) is situated in a healthy part of the forest, while the SCAR plot (Fig. 4c) is located in a forest surface extremely degraded by deer and wild pigs. The plots are limited by steel plates pushed down to a nearly 10 cm depth, but Tramier et al. (2021) showed these plates did not prevent subsurface flow from above the
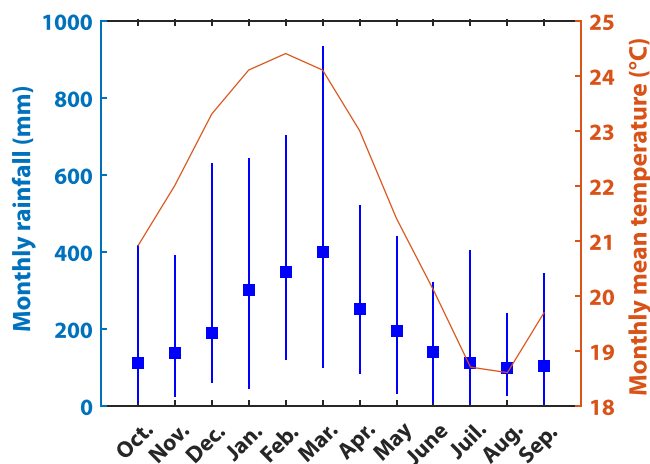

Fig. 2. Mean climate at the Touho airport (5 m altitude) during the 1993–2010 period. Blue squares stand for the mean rainfall and the blue vertical bar for extreme values. The red line represents the mean monthly temperature.

Table 1

Data recorded at the different locations in the HydroThiem observatory (see Fig. 1 for location).

SAV plot	Rainfall, runoff, SMC, soil moisture: 0.2 m depth (top); 0.2 m and 0.6 m depth (bottom of the plot)
REGEN plot	Rainfall, runoff, soil moisture: 0.2 m, 0.45 m, and 0.6 m depth (middle of the plot)
SCAR plot	Rainfall, discharge, SMC, soil moisture: 0.2 m and 0.6 m depth (top and bottom of the plot)
BARR watershed	Discharge
Tiotei	Rainfall
Tipo	Rainfall
CAPT watershed	Discharge, SMC
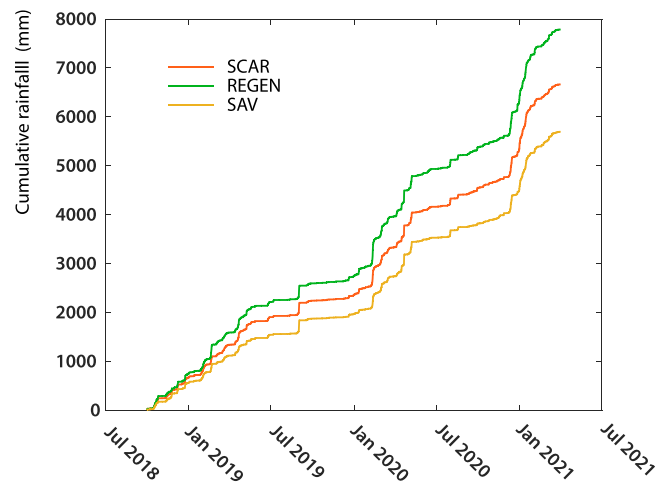
Fig. 3. Comparison of cumulated rainfall observed on the three raingauges presenting a continuous record.

Table 2

Characteristic features of the three plots.

Plot	SCAR	REGEN	SAV
Surface (m^2)	121	85	115
Mean slope (°)	17	19	15
Contributive area above the plot (m^2)	292	0	103
Topographic index (middle of the plot)	5.3	3.2	4.7

Fig. 4. Vegetation at the three plots. a) is SVA, b) is REGEN, c) is SCAR. Note the deer grazing in the SCAR plot (middle right).

plot to enter the plot. Properties of the contributive areas above the plots are also given in Table 2 as well as the Topographic Wetness Indices defined by Beven and Kirkby (1979). The top of the REGEN plot corresponds to a local topographic maximum, so that there is no contributing area above this plot. Water is collected at the base of the plot in a gutter inserted down to a mean depth of 16 cm. It is directed toward a first well, where turbidity is measured then to a 2 m long horizontal channel and to a 244 mm Openchannelfow V-shaped HS Flume weir allowing to measure flow rates ranging from 0.009 to 12.9 dm^3/s according to the manufacturer's specifications. The water height in the weir is measured in a lateral stilling well, with a TE connectivity Trueblue 555 level datalogger presenting a 2 mm accuracy. The channel and the stilling well were levelled each year and we found that a step of maximum height of

9 mm was present at the junction of the stilling well and the pipe bringing water from the channel. Therefore, it was concluded that water levels below 9 mm in the channel could not be measured. According to the table provided by the HS Flume manufacturer, this height of 9 mm corresponds to a flow rate of 0.02 dm^3/s. This effect does not impact the accuracy of measurements of water heights above 9 mm in the weir. The REGEN, SCAR and SAV raingauges were installed less than 200 m away from the corresponding plot in an area devoid of trees. Discharge from the 3 plots are compared in Fig. 5.

3.2.2. Soil moisture

Partitioning of rainfall between runoff and infiltration depends on the water saturation of the superficial soil layers. Soil moisture was explored with Delta-T Thetraprobes ML2x and ML3 installed at depths ranging from 0.2 m to 0.6 m in the three plots. Thetraprobes moisture measurements rely on propagation and reflection of a high frequency (100 MHz) electrical signal between four 6 cm long electrodes inserted in close contact with soil. The Thetraprobes were connected to a GP1 datalogger recording either at a 6 min or at a 15 min time step. Two pairs of probes were installed at the SCAR and SAV plots at mean depths of 0.2 and 0.6 m in the upper and lower part of the plot, while at REGEN three probes were installed at 0.2, 0.45 and 0.6 m depths in the middle of the plot. The calibrations provided by Delta-T for organics soil and for mineral soil were used above and below 0.3 m depth. However unrealistic high moistures where produced during rain events with these calibrations, reaching 0.8, 0.7 and 0.85 at the superficial probes of SCAR, SAV and REGEN, respectively. By comparison, total porosity was measured by the weight difference of soil samples saturated during 12 h in water and oven dried during 24 h. The measured porosity at 0.2 m was 58 % ± 5 % at SCAR, 55 % ± 5 % at SAV and 60 % ± 5 % at REGEN. Therefore moisture data presented here provide only qualitative information on the soil saturation. Some gaps in the dataset result from failure of one probe or of the datalogger and from removal of the electrodes before setting fire at SAV. Comparison of the moisture signal at REGEN, SAV and SCAR is provided in Fig. 6.

3.2.3. Suspended Matter Concentration (SMC) and erosion at the three plots

Suspended matter was measured in the HydroThiem site due to its potential impact on coral species of the lagoon. Suspended sediment transport was also used to compute an estimate of erosion at each plot. Turbidity was measured with a Ponsel NTU sensor using side scattered light in the near infrared domain (880 nm). Using successive dilutions of a concentrated solution, it was determined that these turbidimeters provided a linear relationship between the measured turbidity and SMC up to 1 500 NTU, for the sediments encountered in the HydroThiem site. The time step of the turbidimeters was set to 6 min and reduced to 1 min for a few rain events. Isolated turbidity peaks were observed either at the 6 min or at the 1 min time step. However, when two turbidimeters were placed in the reservoir, these peaks were only observed on one of them. Therefore, they were considered as artifacts resulting from macrosediments (vegetal debris, by example) and replaced by the mean of the previous and the following data points. Moreover, turbidity in the reservoir was no more considered as soon as the flow from the plot stopped. Suspended matter concentration (SMC) was measured from samples collected during two different rain events at the SAV and SCAR plots. Given the low runoff and turbidity
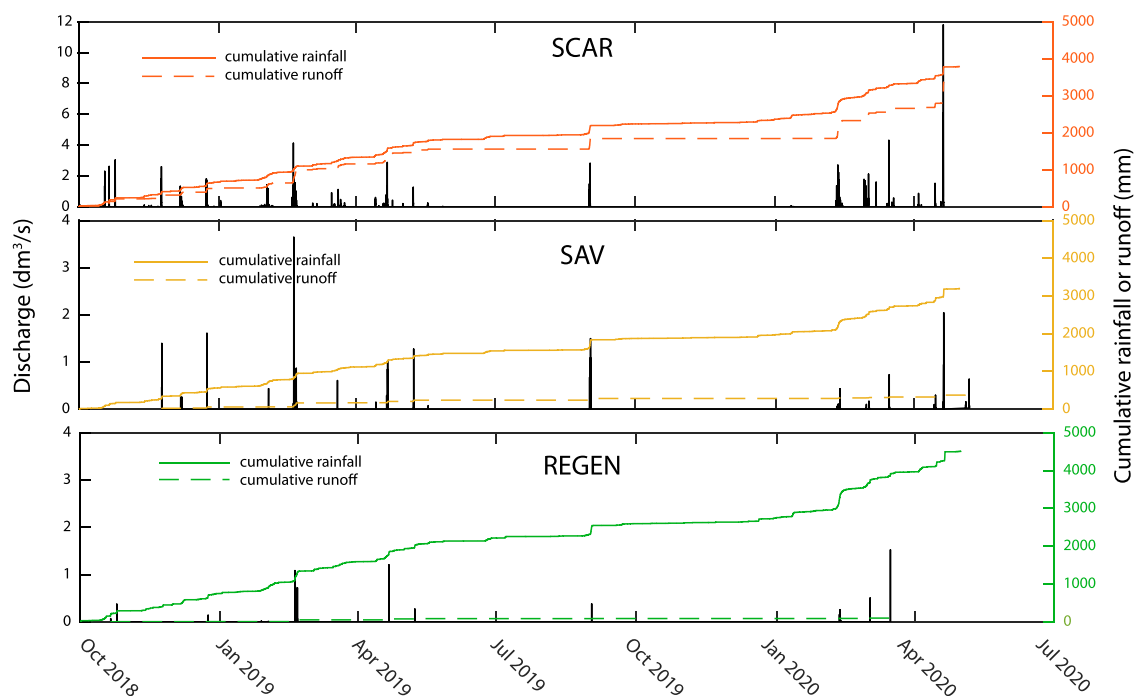
Fig. 5. Discharge observed at the three plots (Oct. 2018–Apr. 2020). Cumulated runoff is also compared to cumulated rainfall (see right scale). Note that the discharge scale is reduced for the two lowest subfigures.
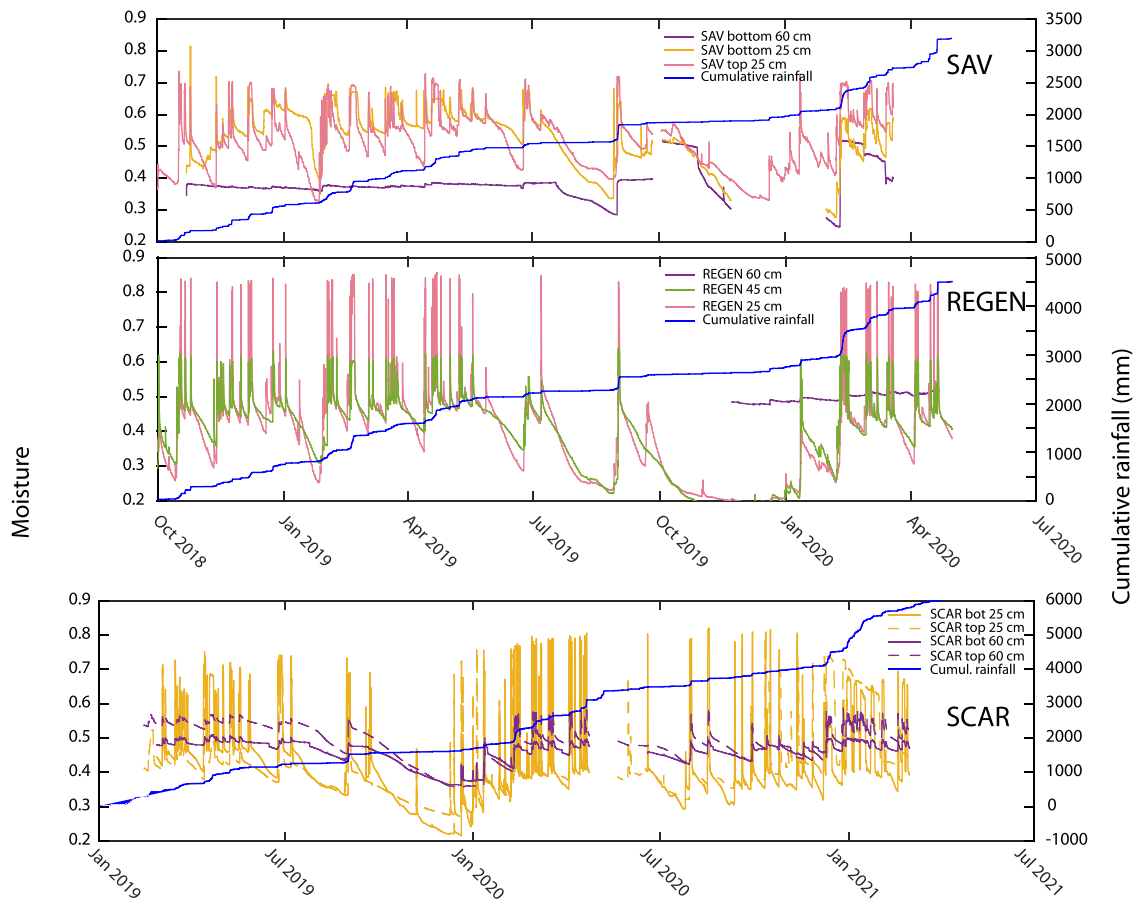
Fig. 6. Comparison of the moisture signal observed at the SAV (top) REGEN (middle) and SCAR (bottom) plots. Cumulative rainfall at the same plot is also pictured. Note that a larger time scale is used for SCAR.

observed at the REGEN plot, it was estimated that this kind of surface produced a negligible amount of suspended matter and the relation between SMC and turbidity was not calibrated there. The following relationships were obtained between SMC (g/m^3) and measured turbidity (Turb in NTU) for the SCAR and SAV plots.

$$SMC\_SCAR = 0.555 \times Turb\_SCAR - 45 \cdot 4 \quad (R^2 = 0 \cdot 99) \tag{1}$$

$$SMC\_SAV = 0 \cdot 285 \times Turb\_SAV + 0.276 \quad (R^2 = 0 \cdot 90) \tag{2}$$

Due to the maximum turbidity observed in our samples, these relationships are valid up to 1 100 NTU at SCAR and to 600NTU at SAV. The corresponding error was computed with a Student law parametrized by the number of turbidity samples (9 for SCAR and 17 for SAV), assuming a 0.95 probability. The mean resulting error on the validity domain of relationships (1) and (2) was 45 gm^{-3} for SCAR and 60 gm^{-3} for SAV. Discharge was interpolated at the turbidity measurement points to produce an erosion rate, computed as the product of discharge and SMC. Maximum and minimum erosion rates resulting from uncertainties on SMC and discharge are provided.

3.3. Runoff and suspended matter at the catchment scale

In order to assess the scale effect on hydrosedimentary properties of characteristic surfaces, runoff was recorded for two watersheds with increasing size (25 200 m^2 and 3.1 km^2) and SMC was measured on the largest one.

3.3.1. The savana watershed (25 200 m^2)

The smallest watershed is called BARR as well its gaging station. It includes mostly woody savanna, was burned once between 2010 and 2020 and its tree cover increased significantly between 1976 and today. It presents a single gully separating two contrasted slopes: the southern and the smallest one (5 200 m^2) presents a 25° mean slope, while the northern one (20,000 m^2) presents a 17.5° mean slope and a larger tree cover. This watershed is equipped with a double rectangular thin plate weir; the upper crest breadth is 1.30 m and its height is 0.345 m, while the lower aperture is 0.3 m wide and 0.15 m high. The lower and upper apertures allow to measure

discharges rates ranging from 0.58 dm^3/s to 31.4 dm^3/s and from 12.5 dm^3/s to 524 dm^3/s, respectively so that the double rectangular weir provides a discharge versus height relationship valid between 0.58 and 556 dm^3/s (Herschy, 2009). The steel plate was inserted in the borders of the gully and perfect sealing between the plate and the gully's banks and bottom was insured by maintaining a thin layer of cement at their junction. No overflow above the border of the outer aperture was observed during the monitoring period. The height versus discharge relationship is the one of the lower weir for a water height in the [0.03–0.15] m range and discharges of the upper weir and of the full lower weir were added for heights larger than 0.18 m. Linear interpolation of these relationships was used for heights lower than 0.03 m or in the [0.15–0.18] m range. Water height was measured with an OTT PLS probe connected to Paratronic Mac 10 R datalogger with an associated accuracy of 1 cm. Discharge errors result from this 1 cm water height error and from a 2 % accuracy estimate for discharge equation of rectangular weirs (Herschy, 2009).

3.3.2. The CAPT watershed (3.1 km^2)

This watershed is mainly constituted of forest presenting a high density and diversity of seedling of the regeneration strata on healthy surfaces, and locally some strong degradations by invasive ungulates. It constitutes half of the surface draining in the Haccinem reservoir which provides drinking water for half of the population of the Touho village. Both the REGEN and SCAR plots are located in the forested part of this watershed. Savana represents 24 % of the surface of this watershed. The CAPT hydrological station is located at base of the watershed, 200 m upstream of the Haccinem reservoir.

3.3.2.1. Rating curve and discharge at CAPT.

The water level is measured with an OTT PLS probe with a 1 cm accuracy in the 0–4 m range and is recorded at a 6 min time step by a Paratronic MAC10R datalogger. Three low flow discharge values were obtained using a mechanical current meter with an assumed error of 10 %. High flow discharges values were computed from two videos including the cross-section where the water level probe is located and where the river bed topography was previously measured. These video records were analyzed according to the LSPIV method (Fujita et al., 1998; Muste et al., 2008) using the discharge (https://discharge.ch) website which produced a pixel/frame image. This image was converted to a superficial velocity image using a two steps method. Firstly the velocity of floating objects within the image was directly measured simultaneously with the video recording, using two markers drawn on both banks of the river. Secondly the observation conditions above the river were exactly reproduced above a grid of regularly spaced ropes and the resulting image was superposed on the pixel/frame image in order to measure geometrical deformations of the pixel/ frame image. Finally total discharge of the river was computed by point integration assuming that the mean velocity on a vertical line was 0.85 times the superficial velocity (Herschy, 2009). There is a large number of possible errors in the LSPIV method and an error of 15 %, in the high range of those proposed in Muste et al. (2008) was assumed. Finally the four gaging points were fitted with a power law relationship, resulting in the following equation:

$$Q = 0·0043 \times H^{2·82} \tag{3}$$

where Q is the discharge rate in dm^3/s and H is the recorded stage in cm. The exponent of 2.82 indicates that Eq. (3) is controlled by a section which lies nearly 20 m downstream the gaging station and where the flow becomes turbulent due to a slope discontinuity (Kennedy, 1984; Herschy, 2009). This equation is accurate only up the highest measured discharge, corresponding to H= 196 cm, while stage values up to 350 cm were recorded. However, there are no slope discontinuities in the river banks up to H = 290 cm so that Eq. (3) provides a fair estimate of discharge at CAPT up to this value. During the studied period, the total discharge above H = 196 cm and H = 290 cm amounted to 8 % and 2 % of the total discharge, respectively.

3.3.2.2. Suspended matter at CAPT.

Turbidity is measured by a Campbell OBS501 dual sensor probe and recorded at a 6 min time step by a Campbell CR300 datalogger. Both turbidity sensors use light emitted in the near infrared domain (850 nm). The sidescatter sensor measures right angle scattered light and is devoted to low turbidities. The backscatter sensor works with light scattered at angles ranging from 125° to 170° from the incident beam and is devoted to measurements of large turbidities. Turbidity data are lacking for a few short time periods resulting from power failures.

Laboratory tests with successive dilutions of a concentrated solution showed that the backscatter sensor provided a linear response up to 1050 FBU. This sensor is best suited for erosion studies. At the 6 min time step, turbidity data from both the sidescatter or the backscatter sensors presented a continuous signal with some isolated peaks which were removed and replaced by interpolation from the previous and the next data point. After correction of these isolated peaks, the maximum recorded turbidity was 820 FBU which lies inside the range of linear response of the backscatter turbidimeter. The relationship between turbidity and SMC was established with 39 samples from three different rain events for the backscatter sensor and with 13 samples of clear water for the sidescatter sensor, resulting in the two following relationships, where SMC is in mg/dm^3 Turb_BS is in FBU units and Turb_SS is in FNU units.

$$SMC\_BS = 2·168 \times Turb\_BS - 78·4 \tag{4}$$

$$SMC\_SS = 0.76 \times Turb\_SS + 5·7 \tag{5}$$

Errors on SMCs computed from Eqs. (4) and (5) were calculated using a Student law parametrized with the number of samples and a 0.95 probability. The mean resulting error on Eqs. (4) and (5) were 30 mg/dm^3 and 10 mg/dm^3, respectively. We noted that although the optical windows was cleaned at each data upload, the minimal observed turbidity was increasing, from 0.2 FNU at the beginning of the data record toward 10 FNU at the end of the record. This results in a low accuracy of the lowest turbidity values. SMC was computed by the SMC_SS equation if Turb_BS < 60 FBU, by the SMC_BS equation if Turb_BS > 80 FBU and by a weighted mean of

SMC_SS and SMC_BS between 60 FBU and 80 FBU, the weight of Turb_BS increasing linearly from zero at 60 FBU to one at 80 FBU. The SM discharge was computed as the product of SMC and discharge interpolated at the SMC measurement points. Maximum and minimum erosion values resulting from errors in discharge and SMC are provided. The SM discharge rate is strongly impacted by uncertainties on the rating curve since highest SMC are observed during highest discharges events. The total amount of SM discharged above h= 196 cm and 290 cm are 45 % and 19 % respectively, so that the largest uncertainties on the rating curve only impact 19 % of the total SM discharge. Cumulative discharge and erosion at CAPT are pictured in Fig. 7.

4. Data availability

Availability of the different data is provided in Fig. 8. Example of most data are shown in Figs. 3, 5, 6 and 7. Data are stored on the Datasud repository site of IRD (https://dataverse.ird.fr). They are included in the HydoThiem directory and metadata are provided. New data will be append as soon as these data become available and checked.

5. Results

Fig. 3 shows that similar rainfalls were observed at the three plots, REGEN receiving most rain. Cumulated rainfall at SCAR and SAV amount to 86 % and 73 % of the one at REGEN on the period displayed on Fig. 3. There is no systematic altitude effect on these three raingauges, which is confirmed if the two additional raingauges Tipo and Tiotei are considered.

Fig. 5 shows that the healthy forest plot (REGEN) corresponds to low runoff (3 % of the incident rainfall on the displayed period) and to dominant infiltration of rainwater, which is a common result in tropical forests (Sidle et al., 2001; Anache et al., 2017). By contrast, the degraded forest plot (SCAR) produces a large runoff amounting to 90 % of the incident rainfall. This high runoff is explained by the several water exfiltration zones observed inside the plot. The SAV plot corresponds to runoff properties intermediate between those of REGEN and SCAR. No significant change in runoff was observed at SAV after the artificial bushfire of Oct. 2019. Tramier et al. (2021) show that the large differences in runoff regimes of the three plots persist if the contributive areas above each plot are considered. However, the absence of any contributive area above the REGEN plot should be considered for interpreting these contrasted runoff coefficients. Indeed, healthy tropical forests are known to produce large subsurface flow (Sidle et al., 2001) and water infiltrating at REGEN can exfiltrate lower in the slope so that healthy forest surfaces could produce significant runoff at the scale of a watershed. Similarly, the large contributive area above SCAR allows a large exfiltration component in the observed runoff and this large runoff could partly explain the degradation at this plot. At the scale of the CAPT watershed, the cumulated rainfall amounts to 5180 mm and the cumulated discharge represents 3380 mm of rainfall during the time period displayed on Fig. 7. This corresponds to a mean runoff coefficient of 64 % and therefore to 36 % of rainfall returning to the atmosphere or being transferred to aquifers and discharged lower in the river or directly to the sea. The resulting maximum ET coefficient is 36 %, which is low for a watershed including 76 % of forest. This is interpreted as resulting from degraded runoff properties of this watershed, water being lost through runoff and not allowed to infiltrate and return to the atmosphere through ET.

In the three plots moisture shows decreasing reaction to rainfall with increasing depth. This is best seen in the REGEN plot, which presents three sensors at 0.20 m 0.45 m and 0.60 m and can be interpreted as a progressive decrease of soil permeability with depth. The two superficial sensors at SAV react strongly to rainfall, the bottom sensor presenting slower drying after rainfall. The bottom deep sensor (60 cm depth) presents a stable moisture near 0.38, a drying during the drought of Aug. and Sep. 2019, and is perturbed since its removal during the artificial fire experiment in Oct. 2019. At SCAR the two superficial sensors present similar behaviors and react to every significant rain event The two deep sensors present a moisture signal characterized by a slightly large mean value and a lower amplitude reaction to rain events, when compared to the superficial ones. They react to the most significant rain events, which could be related to subsurface flow and water exfiltration in this plot.

Cumulated erosion is computed for the three plots during the 2020 rain season, which extended from Feb. 2020 to May 2020. The REGEN plot presents low runoff and sediment load, therefore erosion is negligible at this plot. At SCAR, erosion reaches 26 kg (2.2 $\times$ 10^5 kg/km^2), including 14 kg during the single 12 h event of April 20. During the same time period, 0.6 kg were eroded from the SAV plot, including 0.3 kg for the April 20 event. Hence, erosion at the three plots present still stronger contrasts than runoff. During the time period displayed on Fig. 7, cumulated erosion at CAPT reaches 1.6×10^7 kg including 0.49×10^7 kg (1.6×10^5 kg/ km^2) for the 2020 rain season (1560 mm rainfall) and 1.1×10^7 kg (3.5×10^5 kg/ km^2) for the beginning of the 2020–2021 rain season (2790 mm rainfall). For the 2020 rain season, the erosion rate observed at the scale of the whole CAPT watershed amounts to 72% of the erosion rate observed at SCAR which is one of the most degraded surface of the watershed. Since it can observed on the field that extremely degraded surfaces constitute at most 25% of the watershed, it can be concluded that erosion at the scale of the CAPT watershed includes a large part of gully erosion. This emphasizes the scale effect on erosion in the CAPT watershed. However erosion values presented here cannot be used for estimating long term erosion, since the observation period is too short to include the strongest rain events, which control a significant part of erosion (Nearing et al., 2017).

6. Conclusion

The dataset presented here evidence contrasted hydrosedimentary regimes at a 100 m^2 plot scale between forest and a savanna submitted to a humid tropical climate. Scale effect can be addressed by comparison of results obtained at the plot scale and at the two watersheds. Healthy forest allows infiltration of rainwater, while degraded forest is associated to large runoff. Infiltrated water returns to the atmosphere with ET and promotes a smooth hydrological regime of the Thiem river through subsurface flow. The moderate
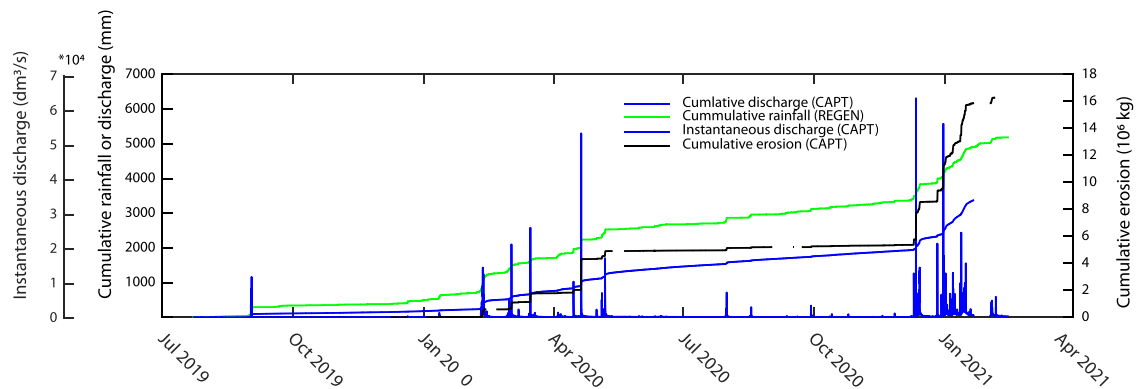
Fig. 7. Cumulative rainfall, discharge and erosion at CAPT. A zero erosion was adopted for missing SMC data and the cumulative erosion curve is interrupted. Instantaneous discharge is also indicated.
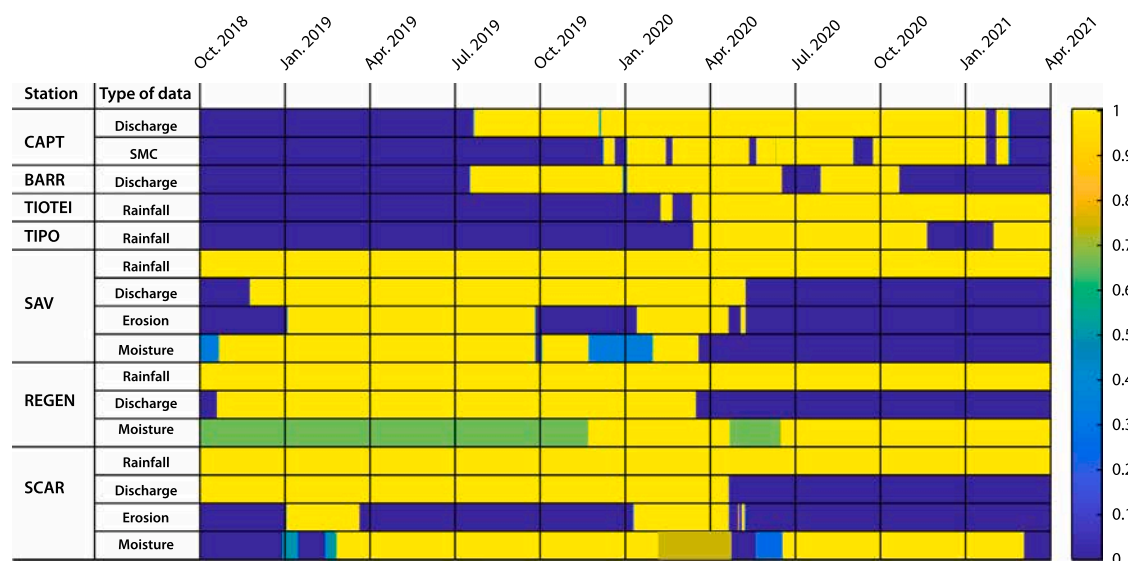
Fig. 8. Data availability between Oct. 1, 2018 and Apr. 1, 2021. Vertical lines correspond to the beginning of each month. Total and partial availability are indicated by the color scale on a daily basis so that yellow stands for 100 % availability and deep blue for no data. Moisture data originate from several probes and partial availability results from failure of one or several probes.

intensity artificial bushfire set up at SAV in Oct. 2019 did not induce a strong change in runoff or erosion. However bushfires may impact the hydrological regime of a watershed by inducing retreating of forests and replacement of forest by savannas. Therefore conservation strategies of watersheds should include regulation of ungulate species in forest and protection of forest/ savanna borders from bushfires. The dataset gathered in the HydroThiem observatory may help fine-tuning of hydrological models such as those of Cerbelaud et al. (2022) or provide a comparison for researchers working on tropical forests and savannas. Moreover, since individual effects of moderate wildfires and of ungulate invasive species are considered in the HydroThiem project, comparison with other degradations, such as deforestation, can be achieved at the 100 m^2 scale as well as at the scale of a small watershed.

Declaration of Competing Interest

The authors declare that they have no known competing financial interests or personal relationships that could have appeared to influence the work reported in this paper.

Data availability

Data are available in repository site (see $4).

Acknowledgements

References

Anache, J.A., Wendland, E.C., Olivera, P.T., Flanagan, D.C., Nearing, M.K., 2017. Runoff and soil erosion plot-scale studies under natural rainfall: a meta-analysis of the Brazilian experience. Catena. https://doi.org/10.1016/jcatena.2017.01.003.

Beven, K.J., Kirkby, M.J., 1979. A physically based, variable contributing area model of basin hydrology. Hydrol. Sci. Bull. https://doi.org/10.1080/02626667909491834.

Cerbelaud, A., Lefevre, J., Genthon, P., Menkes, C., 2022. Assessment of the WRF-Hydro uncoupled hydro-meteorological model on flashy watersheds of the Grande Terre tropical island of New Caledonia (South-West Pacific). J. Hydrol. Reg. Stud. https://doi.org/10.1016/j.ejrh.2022.101003.

Davis, N.E., Bennett, A., Fossyth, D.M., Bowman, D.M., Lefroy, E.C., Wood, S.W., Woolnough, A.P., West, P., Hampton, J.O., Jordan, O., Johnson, C.N., 2016. A systematic review of the impacts and management of introduced deer (family Cervidae) in Australia. Wildl. Res. https://doi.org/10.1071/WR16148.

Dumas, P., Toussaint, M., Herrenschmidt, J.-B., Conte, A., Mangeas, M., 2013. Bushfire risk in Grande Terre of New Caledonia: humans responsible but not guilty. Rev. Geogr. Est. https://doi.org/10.4000/rge.4598.

Duncombe, J., 2020. Five environmental consequences of Australia's fires. Eos 101. https://doi.org/10.1029/2020EO138596.

Ebel, B.A., Moody, J.A., Martin, D.A., 2022. Post-fire temporal trends in soil-physical and hydraulic properties and simulated runoff generation: Insights from different burn severities in the 2013 Black Forest Fire, CO, USA. Sci. Total Environ. https://doi.org/10.1016/j.scitotenv.2021.149847.

Fujita, I., Muste, M., Kruger, A., 1998. Large-scale particle image velocimetry for flow analysis in hydraulic engineering applications. J. Hydraul. Res. https://doi.org/10.1080/00221689809498626.

de Garine-Wichatitsky, M., de Meeûs, T., Chevillon, C., Berthier, D., Barré, N., Thévenon, S., Maillard, J.-C., 2009. Population genetic structure of wild and farmed rusa deer (*Cervus timorensis rusa*) in New-Caledonia inferred from polymorphic microsatellite loci. Genetica. https://doi.org/10.1007/s10709-009-9395-6.

Herschy, R.W., 2009. Streamflow Measurement. Taylor & Francis, NY, USA.

Ibanez, T., Borgniet, L., Mangeas, M., Gaucherel, C., Géraux, H., Hély, C., 2013. Rainforest and savanna landscape dynamics in New Caledonia: towards a mosaic of stable rainforest and savanna states? Austral Ecol. https://doi.org/10.1111/j.1442-9993.2012.02369.x.

Kennedy, E.J., 1984. Discharge Rating at Gaging Stations, USGS Techniques of Water Resources Investigations (ch. 10).. USGS, Menlo Park, CA.

Lachassagne, P., Dewandel, B., Wyns, R., 2021. Groundwater in granitic and metamorphic rocks. Encycl. Environ. ⟨https://www.encyclopedie-environnement.org/en/water/groundwater-in-granitic-and-metamorphic-rocks/⟩.

Maitrepierre, L., 2012. Les types de temps et les cyclones, les éléments du climat. In: Bonvallot, J., Gay, J.-C. (Eds.), Atlas de la Nouvelle Calédonie. IRD, Marseille France.

Martin, J.-L., Baltzinger, C., 2002. Interactions among deer browsing, hunting and tree regeneration. Can. J. For. Res. 32, 1254–1264.

Mataix-Solera, J., Cerdà, A., Arcenegui, V., Jordán, A., Zavala, L.M., 2011. Fire effects on soil aggregation: a review. Earth Sci. Rev. https://doi.org/10.1016/j.earscirev.2011.08.002.

Maurizot, P., Cluzel, D., Patriat, M., Collot, J., Iseppi, M., Lesimple, S., Secchiari, A., Bosch, D., Montanini, A., Macera, P., Davies, H.L., 2020. The eocene subduction-obduction complex of New Caledonia. In: Maurizot, P., Mortimer, N. (Eds.), New Caledonia: Geology, Geodynamic Evolution and Mineral,. Geological Society Memoir No. 51. The Geological Society, London. https://doi.org/10.1144/M51-2018-70.

Moody, J.A., Ebel, B.A., Nyman, P., Martin, D.A., Stoof, C.R., McKinley, R., 2016. Relation between soil hydraulic properties and burn severity. Int. J. Wildland Fire. https://doi.org/10.1071/WF14062.

Moody, J.A., Shakesby, R.A., Robichaud, P.R., Cannon, S.H., Martin, D.A., 2013. Current research issues related to post-wildfire runoff and erosion processes. Earth Sci. Rev. https://doi.org/10.1016/j.earscirev.2013.03.004.

Murphy, B.P., Bowman, D.M.J.S., 2012. What controls the distribution of tropical forest and savanna? Ecol. Lett. https://doi.org/10.1111/j.1461-0248.2012.01771.x.

Muste, M., Fujita, I., Hauet, A., 2008. Large-scale particle image velocimetry for measurements in riverine environments. Water Res. Res. https://doi.org/10.1029/2008WR006950.

Nakagawa, H., 2021. Comparison of macroinvertebrate assemblages in a stream before and after fine sedimentation by deer-induced forest floor degradation. Ecol. Res. https://doi.org/10.1111/1440-1703.12256.

Nearing, M.A., Xie, Y., Liu, B., Ye, Y., 2017. Natural and anthropogenic rates of soil erosion. Int. Soil Water Conserv. Res. https://doi.org/10.1016/j.iswcr.2017.04.001.

Sidle, R.C., Noguchi, S., Tsuboyama, Y., Laursen, K., 2001. A conceptual model of preferential flow systems on forested hillslopes: evidence of self-organization. Hydrol. Process. https://doi.org/10.1002/hyp.233.

Stavi, I., 2019. Wildfires in grasslands and shrublands: a review of impacts on vegetation, soil, hydrology, and geomorphology. Water. https://doi.org/10.3390/w11051042.

Toussaint, M., 2020. Are Bush fires and drought 'natural disasters'? The naturalisation of politics and politicisation of nature in New Caledonia. Anthropol. Forum. https://doi.org/10.1080/00664677.2019.1647829.

Tramier, C., Genthon, P., Delvienne, Q., Sauvan, N., Cassan, J.-J., Ebrard, E., Dumas, P., Queffelean, Y., 2021. Hydrological regimes in a tropical valley of New Caledonia (SW Pacific): impacts of wildfires and invasive fauna. Hydrol. Proc. https://doi.org/10.1002/hyp.14071.

Viera, D.C., Fernandez, C., Vega, J.A., Keizer, J.-J., 2015. Does soil burn severity affect the post-fire runoff and interrill erosion response? A review based on meta-analysis of field rainfall simulation data. J. Hydrol. https://doi.org/10.1016/j.jhydrol.2015.01.071.